ISSN 1936-878X/09/$36.00
PUBLISHED BY ELSEVIER INC.
DOI:10.1016/j.jcmg.2009.04.003

iREVIEWS

STATE-OF-THE-ART PAPER

Quantification of Absolute Myocardial Blood Flow by Magnetic Resonance Perfusion Imaging

Daniel C. Lee, MD, Nils P. Johnson, MD

Chicago, Illinois

By serially imaging the myocardium during the initial transit of gadolinium contrast, magnetic resonance perfusion imaging can accurately assess relative reductions in regional myocardial blood flow and identify hemodynamically significant coronary artery disease. Models can be used to quantify myocardial blood flow (in milliliters/minute/gram) on the basis of dynamic signal changes within the myocardium and left ventricular cavity. Although the mathematical modeling involved in this type of analysis adds complexity, the benefits of absolute blood flow quantification might improve clinical diagnosis and have important implications for cardiovascular research. (J Am Coll Cardiol Img 2009;2:761–70) © 2009 by the American College of Cardiology Foundation

Although coronary angiography remains the standard for diagnosing coronary artery disease (CAD), visual estimates of stenosis severity and hemodynamic significance remain imperfect (1). Intracoronary assessments of pressure gradients and flow reserve involve greater procedural risk and higher cost than noninvasive techniques.

Positron emission tomography (PET) has traditionally been the noninvasive standard for quantitative measurements of absolute myocardial blood flow (AMBF) in milliliters/minute/gram. Measurements at stress and rest have been reported in normal individuals, and reductions in myocardial perfusion reserve (MPR) have been demonstrated in patients with CAD risk factors (2). However, widespread clinical application has been slowed by limited access to cardiac PET cameras and short-lived radiopharmaceuticals. PET imaging also involves exposure to ionizing radiation, and the low spatial resolution limits evaluation of transmural flow differences in normal thickness myocardium.

Single-photon emission computed tomography images are scaled to the most intense area of uptake in the ventricle, enabling assessment of relative perfusion but not absolute perfusion or MPR. AMBF quantification is possible with dynamic single-photon emission computed tomography imaging (3), but cameras with sufficient speed and count sensitivity are not widely available. Myocardial contrast echocardiography enables real-time, bedside measurement of parameters reflecting blood velocity and blood volume, the product of which provides an index of perfusion and MPR (4). However, the quality of regional intensity time

From the Feinberg Cardiovascular Research Institute, Department of Medicine and Division of Cardiology, Bluhm Cardiovascular Institute, Feinberg School of Medicine, Northwestern University, Chicago, Illinois. This work was supported by an award from the American Heart Association, the Northwestern Memorial Foundation, the Feinberg Cardiovascular Research Institute, and the Department of Medicine, Northwestern University Feinberg School of Medicine. Dr. Lee has received research grant support from St. Jude Medical (significant) and consulting fees from St. Jude Medical (modest) and Siemens Medical Solutions (modest).

Manuscript received December 31, 2008; revised manuscript received March 24, 2009, accepted April 13, 2009.

JACC: CARDIOVASCULAR IMAGING, VOL. 2, NO. 6, 2009
JUNE 2009:761–70

courses might be compromised by limited windows or shadowing from blood signal, and obtaining an arterial input function suitable for modeling remains difficult. Computed tomography perfusion can quantify AMBF (5) with models similar to those described in the following text. Limitations include the need for both ionic contrast and radiation exposure in addition to modality-specific artifacts due to beam hardening.

Cardiac magnetic resonance perfusion imaging (CMR-PI) can quantify AMBF in milliliters/minute/gram. Some advantages of CMR-PI include its lack of ionizing radiation, the wide availability of CMR imaging systems, and a sufficiently high spatial resolution to allow analysis of transmural differences in myocardial blood flow. This article will begin by briefly reviewing the steps involved in acquiring CMR-PI studies and the clinical performance of qualitative and semiquantitative analysis of CMR-PI studies. The majority of this article will focus on the theory and experimental results supporting CMR-PI quantification of AMBF.

ABBREVIATIONS AND ACRONYMS

AMBF = absolute myocardial blood flow

CAC = coronary artery calcium score

CAD = coronary artery disease

CMR-PI = cardiac magnetic resonance perfusion imaging

FFR = fractional flow reserve

GdCA = gadolinium-based contrast agent

LGE = late gadolinium enhanced

LSI = linear, shift-invariant

LV = left ventricular

MPR = myocardial perfusion reserve

SNR = signal-to-noise ratio

TIC = time intensity curve

CMR-PI Acquisition

Most CMR-PI studies are performed in a clinical 1.5-T magnet with phased array receiver coils placed on the chest and back. The heart is imaged every cardiac cycle during the passage of an intravenous bolus of a gadolinium-based contrast agent (GdCA). Because gadolinium is a paramagnetic compound that decreases T1 relaxation times, regional delivery of GdCA-rich blood results in a progressive increase in signal intensity on T1-weighted pulse sequences. Areas receiving impaired blood flow and consequently less GdCA appear darker than normally perfused areas (Fig. 1). Imaging during pharmacologic vasodilation with adenosine or dipyridamole is routinely performed to improve the differentiation of normal from stenotic perfusion beds. A typical clinical perfusion study also includes resting cine and late gadolinium enhanced (LGE) images. Cine CMR provides reproducible, high-resolution assessment of cardiac mass, volume, and function. LGE accurately defines the location and extent of acute and chronic infarction and predicts the likelihood of wall motion recovery after revascularization (6). Imaging time for a full study is approximately 50 min.

Qualitative and Semiquantitative Analysis

The simplest method for interpreting CMR-PI studies is to view the study in cine-loop format for regions of relative hypoperfusion. Numerous single center studies demonstrate high diagnostic accuracy when qualitative interpretation of clinical CMR-PI studies is compared with invasive angiography (7).

Figure 1 depicts semiquantitative analysis of a CMR-PI study, which examines the mean signal intensity within a region of interest over time, or "time intensity curve" (TIC). Measurements such as the maximum upslope or initial area under the TIC have been used as indexes of regional flow (8). In animals these indexes have been shown to correlate well with flow measurements based on injected microspheres (9,10). Semiquantitative analysis has been shown to improve diagnostic accuracy over visual analysis alone (11).

Early results regarding the prognostic value of CMR-PI indicate that patients with an abnormal perfusion study have a higher incidence of cardiac death or nonfatal myocardial infarction than those with a normal scan, and patients with a normal scan have an annual hard event rate of <1% per year (12)—similar to the prognosis of a normal radionuclide perfusion scan (13).

Absolute Perfusion Quantification

In contrast to semiquantitative methods, models exist that quantify AMBF. These are similar in derivation to those employed in quantitative PET and computed tomography perfusion as well as thermodilution estimation of cardiac output. Flow models use the myocardial and left ventricular (LV) blood pool TICs to estimate AMBF. Although a detailed mathematical description of these flow models is beyond the scope of this review, some understanding of their assumptions and limitations can guide their appropriate application. Two major classes of models exist: linear, shift-invariant (LSI) models and compartment models. Each class of model has its own assumptions that must hold or at least approximately hold for the model to produce meaningful and valid estimations of flow.

LSI models. The LSI models have proved more popular in CMR-PI than compartment models. The LSI models assume the cardiac circulatory system is linear and temporally invariant in its response. In other words, if 2 contrast boluses are injected, then the myocardial uptake is the linear sum of the uptake had each bolus been injected separately; and if the injection of a bolus is delayed

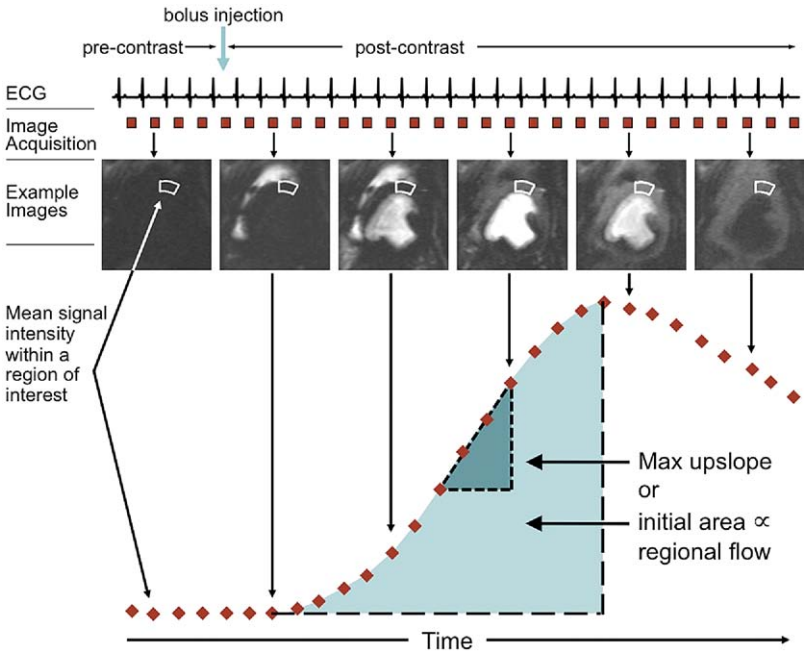

Figure 1. CMR-PI Acquisition and Semiquantitative Analysis

The heart is imaged every cardiac cycle during the first passage of gadolinium-based contrast agent. The resulting 30- to 40-frame image stack can be viewed in cine-loop format for qualitative assessment of regional flow deficits. Semiquantitative flow analysis involves measuring the mean signal intensity over time for a region of interest and calculating the peak upslope or area under the curve as an index of regional flow. Adapted with permission from Lee et al. (54). CMR-PI = cardiac magnetic resonance perfusion imaging; ECG = electrocardiogram.

by a certain amount of time, then its uptake is delayed (shifted) by the same amount of time. These 2 assumptions allow for a powerful and complete description of the system by its so-called "transfer function." Characteristics of the transfer function reflect properties of its system, the most relevant of which is AMBF.

The output from an LSI system (the myocardial TIC) is equal to the input to the system (the tracer bolus, measured from the LV TIC) merged with the transfer function by a mathematical process known as convolution (Fig. 2). Convolution folds 2 curves together via a shift-scale-and-add process similar to cross-correlation in statistics. To obtain the transfer function, the input and output curves must undergo the reverse process of deconvolution. Unfortunately the process of deconvolution is very sensitive to noise, so that small errors in the input data can lead to large differences in the resulting transfer function. Therefore, additional constraints need to be imposed to obtain a physiologic solution.

The most popular method for "constrained" deconvolution demands that the transfer function take a certain shape. This curve can be described by 4 parameters and is known as the Fermi function (14) (Fig. 2). It can be shown that the maximum value of the Fermi transfer function equals AMBF (15). Note that the Fermi function builds in a delay before its upstroke to allow for passage of the contrast from the left ventricle into the coronary arteries before perfusing the tissue.

The validity of deconvolution depends most importantly on the assumption of linearity. Both the input (signal in the LV blood pool) and output (signal in the myocardium) must behave in the same linear fashion with the concentration of tracer. To maximize the signal-to-noise ratio (SNR) in the myocardium, a large gadolinium bolus is preferred. However, at clinically desired myocardial signals, the linear range of the CMR signal response within both the blood pool and myocardium has already been exceeded.

This nonlinear effect within the LV blood pool has been appreciated for many years. Two techniques have been proposed to preserve both high myocardial SNR and linear blood pool signal response. The dual-T1 sensitivity technique (16) acquires both low-resolution, low T1-sensitivity blood pool and high-resolution, high T1-sensitivity myocardial data within each R-R interval. The dual-bolus

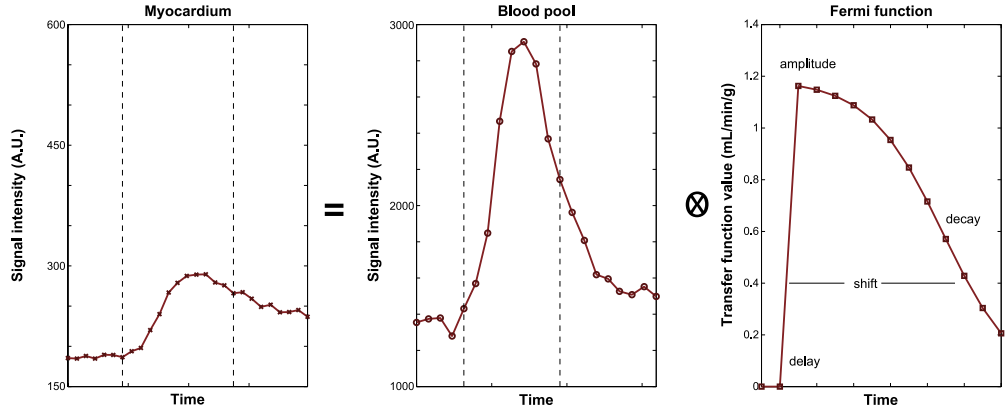

Figure 2. AMBF Calculation by Fermi Function Deconvolution

Myocardial time intensity curve (TIC) **(left-most panel)** equals the blood pool TIC **(middle panel)** convolved with **("X" symbol in circle)** the Fermi transfer function **(right-most panel)**. The maximum amplitude of the transfer function equals absolute myocardial blood flow (AMBF). In this data from a dual-bolus study, the blood pool signal intensity (SI) values from the minibolus have been magnified by a factor of 10 on the basis of the gadolinium (Gd) concentration ratio of the mini and full bolus (0.005/0.05 mmol/kg). The areas between the **dashed lines** of the myocardial and blood pool TICs are used for analysis; these underwent correction for coil effects and baseline SI, then conversion to Gd concentration before deconvolution. A.U. = arbitrary units.

technique (17) injects 2 boluses, an initial minibolus that maintains blood pool linearity followed by a large bolus that maximizes myocardial SNR (18).

It had been assumed, because myocardial CMR signals were much less than blood pool signals, that nonlinearity was not an issue within the myocardium. However, a growing body of evidence suggests that myocardial nonlinearity becomes significant at bolus concentrations necessary for sufficiently high myocardial SNR (19–21). This effect might be due to incomplete extraction of GdCA from the vascular space, limiting the proportion of myocardial protons with which gadolinium can interact. The optimal solution to this nonlinearity has not yet been defined, although converting the CMR signal into gadolinium concentration (19,21) or correcting the signal with algorithms based on the theoretical signal response to gadolinium (22,23) might be feasible options.

Another assumption in the LSI model is that the input function can be accurately measured. For convenience, the input TIC is taken from the LV blood pool in the short axis. However, this bolus undergoes further mixing and dispersion before reaching the coronary arteries, a phenomenon better appreciated in quantitative cerebral perfusion (24). Additionally, the presence of collateral flow alters the input function seen by a region of myocardium (25). These effects need to be minimized or accounted for when specifying the input time-intensity curve.

The specific validity of the Fermi deconvolution model is challenged by several deviations from its assumptions. First, the tracer bolus recirculates, and thus its "first-pass" contains some of the second-pass as well. Although recirculation does not violate the assumptions of an LSI system, it does demand a more complex transfer function than that offered by the Fermi model. Alternatively, recirculation can be modeled and subtracted from the time-intensity curves to remove its effects (26). Second, most clinically approved GdCA do not remain exclusively within the intravascular space, but leak into extravascular compartments. Again, this leak does not violate LSI assumptions, but the Fermi transfer function cannot accommodate it. Finally, the presence of collaterals requires a more complex shape to the transfer function than allowed by the Fermi model (25).

To overcome these limitations, a more complex constrained deconvolution model termed "model-independent" (although it is itself a parameterized model) has been proposed (27). This builds a transfer function from splines and uses sophisticated mathematical techniques to produce a more intricate curve while not overfitting noise within the data. However, its use has not become widespread, likely due to its mathematical complexity.

Compartment models. Compartment models divide the cardiac circulatory system into distinct spaces (intravascular, interstitial, and intracellular). The GdCA concentration varies among these compartments over time as molecules move from 1 space to another. Rate constants describe the movement between any 2 compartments (Fig. 3). Such models determine compartment concentrations and the

individual rate constants from the summed time-intensity curve of all compartments (28).

Current Food and Drug Administration-approved GdCAs leak from the intravascular compartment into the interstitial compartment along an osmotic gradient but do not enter the intracellular compartment. Thus, a 2-compartment model (intravascular and interstitial) has been used to model its transit through the cardiac circulatory system (19). The solution to the differential equations describing this 2-compartment model also produces a convolution relationship. In this case, the transfer function is an exponential decay. There are 2 parameters to the 2-compartment model's transfer function. Unlike the LSI model, for which the maximum amplitude of its transfer function is equal to AMBF, the maximum amplitude of the 2-compartment model transfer function is equal to the product of AMBF and the myocardial extraction efficiency of the contrast agent. Their product is labeled "k_1" (the first-order rate constant) by many authors when reporting their results. If the extraction efficiency is known or can be estimated, then AMBF alone can be determined. However, this adds an extra assumption to the model for quantifying perfusion. Thus, an advantage of the LSI model is that AMBF can be calculated explicitly, provided the transfer function can account for the extravascular leakage of contrast (e.g., model independent). The 2-compartment model also depends on linearity of signal response, so the previous comments about ensuring linearity in the blood pool and myocardium apply as well.

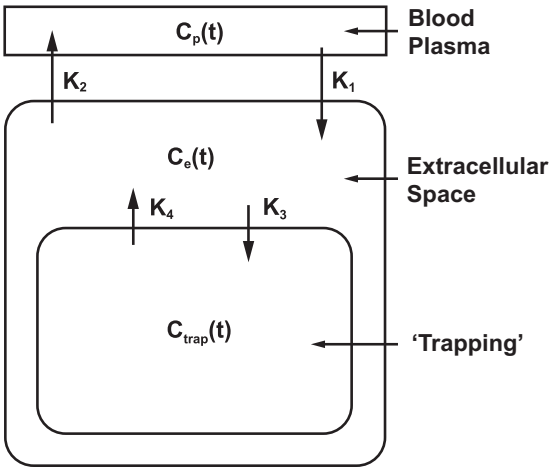

Figure 3. Diagram of a 3-Compartment Model

Divisions are illustrated for the blood plasma (p), extracellular space (e), and a trapped intracellular space (trap). $C_p(t)$, $C_e(t)$, and $C_{trap}(t)$ represent the gadolinium (Gd) concentration change over time in each compartment, and K_1, K_2, K_3, K_4 represent the transfer rate of Gd between compartments (reprinted with permission from Fig. 1 of Knowles et al. [56]).

Validation of Absolute Perfusion by CMR-PI in Animal Models

Several studies have evaluated perfusion in instrumented animals to compare noninvasive AMBF by CMR-PI (17,18,21,27,29) with flow measured by injected microspheres, which provide a pathologic gold standard for regional tissue perfusion (30). Synthesizing the results from these studies is somewhat difficult because of important differences in CMR pulse sequence, bolus strategy, quantitative model, and application of myocardial signal nonlinearity correction (Table 1). Averaging adjacent slices (27) or restricting analysis to stenotic and remote zones (excluding sectors in shoulder regions) (17,29) might also reduce errors of registration between CMR and microsphere flow. Methodological differences notwithstanding, the overall correlation between CMR and microsphere AMBF is good to excellent, with the correlation coefficient ranging from 0.79 to 0.95 over a wide range of myocardial blood flows. Additionally, absolute perfusion correlated more closely with microsphere blood flow than established semiquantitative CMR indexes. When the same signal intensity–time curves were analyzed to calculate the peak enhancement ratio, upslope index, and area under the curve, these indexes plateaued at higher blood flows, resulting in significant underestimation of microsphere flow values (17).

The existing body of experimental published data in which AMBF by CMR-PI with LSI models and microspheres are compared in milliliters/minutes/gram is still rather limited (total number of analyzed segments 388) (Table 1). Also, lack of consensus on optimal acquisition and analysis techniques limits broad application at the present time.

Additional studies employing LSI models have shown a good correlation between CMR and microsphere-determined MPR but did not report AMBF (31,32). Experimental studies using a compartment model have also demonstrated a linear relationship between k_1 and microsphere-derived AMBF over a flow range of <1 ml/min/g ($r = 0.88$) (33), but changes in extraction efficiency at higher flow rates might affect this relationship.

Absolute Perfusion Quantification in Normal Volunteers

Understanding AMBF in normal individuals is essential for appropriate evaluation of disease states.

JACC: CARDIOVASCULAR IMAGING, VOL. 2, NO. 6, 2009
JUNE 2009:761–70

Table 1. Experimental Studies Comparing AMBF by CMR-PI and Injected Microspheres

Author, Year (Ref. #)	CMR-PI Studies	# of Sectors	GdCA Bolus (mmol/kg)	AMBF Range (ml/min/g)	Pulse Sequence	Transfer Function	Linear Correlation
Jerosch-Herold, 2002 (27)	5 studies (3 pigs)	30–40	Single (0.04)	0.5–>6	SR-FLASH	Model independent	y = 0.96x + 0.06 r = 0.96
Mühling, 2003 (29)	24 studies (12 pigs)	46	Single (0.03)	0–>2.5	SR-FLASH	Fermi function	y = 0.77x + 0.11 r = 0.79
Christian, 2004 (17)	16 studies (16 dogs)	96	Dual (0.0025/0.1)	0–>5	SR-EPI	Fermi function	y = 0.95x + 0.1 r = 0.95
Lee, 2008 (21)*	14 studies (4 dogs)	84	Dual (0.005/0.05)	0–4	SR-EPI	Fermi function	y = 0.93x - 0.05 r = 0.82
Christian, 2008 (18)	12 studies (6 dogs)	36	Dual (0.0025/0.1)	0.5–4.5	SR-EPI	Fermi function	r = 0.94
		36	Single (0.025)				r = 0.91

*Signal intensity–time curves were converted to gadolinium concentration-time curves before deconvolution.
AMBF = absolute myocardial blood flow; CMR-PI = cardiac magnetic resonance perfusion imaging; GdCA = gadolinium-based contrast agent; SR-FLASH = saturation recovery fast low angle shot; SR-EPI = saturation recovery gradient-echo with echo-planar readout.

Resting and vasodilated AMBF have been evaluated by CMR-PI in small cohorts of healthy volunteers (Table 2) (34,35). Overall, CMR-PI AMBF measurements are in agreement with published values based on invasive (36) and noninvasive methods (2), and the magnitude of flow heterogeneity (34) is similar to that seen in PET (37).

Absolute Perfusion Quantification in Patients With Epicardial Coronary Artery Stenoses

Investigators have begun to explore whether the improved accuracy of AMBF over qualitative and semiquantitative techniques demonstrated in animal models would translate to patients with suspected CAD undergoing coronary angiography (38). An MPR cutoff of 2.04 was 93% sensitive and 57% specific in predicting intracoronary fractional flow reserve (FFR) ≤0.75 and 85% sensitive and 49% specific in predicting ≥50% diameter stenosis by quantitative coronary angiography. The authors suggested that low specificity might be due to microvascular dysfunction causing low MPR in segments with preserved FFR or low diameter stenosis. In the same group of patients, quantitative MPR performed better than semiquantitative or visual techniques (39). The optimal MPR cutoff value is higher than cutoff values derived from previous studies of relative perfusion (40), which might be due to underestimation of AMBF at higher flow rates by semiquantitative methods (17).

Table 2. AMBF by CMR-PI Measured in Healthy Volunteers

Author, Year (Ref. #)	Rest AMBF (ml/min/g)	Stress AMBF (ml/min/g)	Perfusion Reserve
Muehling, 2004 (34)	1.1 ± 0.4	4.2 ± 1.1	4.1 ± 1.4
Hsu, 2006 (35)	1.0 ± 0.2	3.4 ± 0.6	3.4 ± 0.7

Abbreviations as in Table 1.

Global Reductions in MPR

AMBF might be particularly advantageous in patients with globally reduced MPR, because qualitative or semiquantitative methods might be hampered by the lack of a normal reference segment. In patients with chest pain and without hemodynamically significant coronary artery lesions (a.k.a. "Syndrome X"), a close linear correlation has been shown between MPR by CMR-PI and intracoronary flow reserve (15,32). In patients with hypertrophic cardiomyopathy, hyperemic AMBF was significantly lower than in control subjects and remained so even after adjusting for end-diastolic wall thickness (41). A stepwise reduction in MPR and endo/epicardial perfusion ratio was demonstrated when comparing volunteers, transplant recipients with no hypertrophy or prior rejection, transplant recipients with either hypertrophy or prior rejection, and transplant recipients with transplant arteriopathy (42).

Hyperemic AMBF and MPR have also been shown to correlate inversely with risk factor burden for coronary heart disease in a population-based cohort of asymptomatic adults (43). When stratified according to coronary artery calcium score (CAC), mean resting AMBF did not differ across CAC levels, but mean hyperemic AMBF and MPR were progressively lower across increasing CAC levels (44). A subset of these patients also underwent tagged cine CMR examination, demonstrating that lower hyperemic MBF was associated with reduced regional peak systolic circumferential strain in the right coronary artery and left circumflex coronary artery regions (45).

Disease Progression/Response to Therapy

AMBF might also be advantageous in monitoring disease progression or perfusion changes in response to therapy, because (unlike measurements of relative regional perfusion) changes in the test and remote regions can be considered separately. Because the limits of agreement between CMR-PI and microsphere AMBF are approximately ± 0.6 ml/min/g (17), detection of individual changes in resting or peri-infarction flow might not be possible. However, detecting changes in vasodilated flow might be possible, and studies that have evaluated group differences in resting and vasodilated AMBF are discussed in the following text.

The CMR-PI performed before and 6 weeks after implantation of a device designed to induce angiogenesis in pigs reported an increase in adenosine vasodilated AMBF in the treated area, which was not seen in sham animals (46). The AMBF measured before and after transmyocardial laser revascularization in a pig model of ischemia reported preserved AMBF in transmyocardial laser revascularization-treated animals but reduced AMBF in untreated animals (29).

In patients with hibernating myocardium, hibernating segments had reduced resting AMBF before percutaneous coronary intervention (PCI), which was lower than in remote segments. AMBF increased in revascularized segments to levels comparable to remote segments after PCI, and improvement in regional wall motion accompanied increases in AMBF (47). In a study of patients with CMR evidence of distal embolization after PCI, segments demonstrating new distal LGE had a fall in MPR from the pre-PCI scan to 24 hours after PCI, whereas MPR in segments without LGE increased. In patients who were scanned 6 months later, MPR in affected segments normalized (48).

Measurement repeatability importantly influences power calculations in studies attempting to detect changes after an intervention. In 7 normal volunteers and 9 patients with CAD undergoing CMR-PI, the coefficient of variation for global MPR was 21% for AMBF and 41% for semiquantitative upslope analysis (49). In 30 participants of the MESA (Multi-Ethnic Study of Atherosclerosis) study who underwent 2 CMR exams approximately 1 year apart, the absolute repeatability coefficient as a percentage of mean blood flow was 30% at rest and 41% during hyperemia (50)—similar to studies of PET performed at rest (27% of mean) (51) and higher than PET values reported at stress (25% of mean) (52), although these PET studies were performed 1 h apart in a younger cohort with higher vasodilated AMBF.

Subendocardium

The sensitivity for detecting limitations in myocardial perfusion might be improved by measuring flow in the subendocardium, where hemodynamic factors and the impact of microvascular dysfunction are more prominent (53). The high spatial resolution of CMR-PI has been used to assess the gradient in flow from endocardium to epicardium (54,55) (Fig. 4). With absolute perfusion techniques, endocardial flow was reduced in comparison with epicardial flow in dog models of coronary artery stenosis (17,21). In healthy volunteers, mean perfusion in the endocardium was significantly higher than in the epicardium at rest but similar during stress (34). And in patients with hypertrophic cardiomyopathy, the likelihood of an endomyocardial/epimyocardial MBF ratio <1 during hyperemia increased with wall thickness (41).

Patient Selection

Contraindications to CMR include certain implanted medical devices (including pacemakers) and medical conditions (unstable angina or New York Heart Association functional class IV heart failure). GdCA should not be administered to pregnant and lactating women or patients with severe renal disease (glomerular filtration rate <30 ml/min/1.73 m^2). Finally, the usual contraindications to adenosine administration (advanced heart block, respiratory compromise) apply.

Study Limitations and Future Directions

Further advancements need to continue both in CMR-PI acquisition and AMBF analysis. Most contemporary pulse sequences do not achieve full heart coverage but can acquire at least 3 short-axis slices every heart beat with an acquisition time of approximately 150 ms/slice and a spatial resolution of <2 mm. Faster pulse sequences, new acceleration techniques, and imaging at higher field strengths should enable greater heart coverage, spatial resolution, and/or contrast-to-noise ratio.

The AMBF models continue to be refined to balance the complexity of the model against susceptibility to noise. Direct comparisons of different analysis schemes are beginning to emerge (18) and should help define the most appropriate analytic technique.

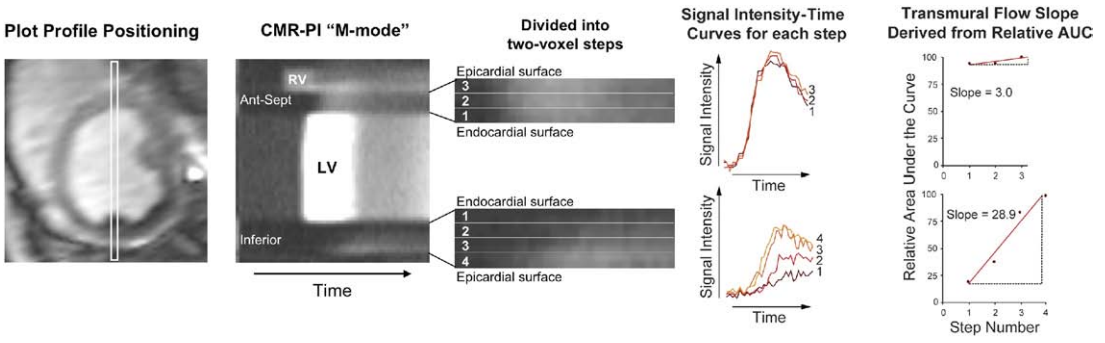

Figure 4. Transmural Gradient in Flow Measured by CMR-PI

The relative gradient in flow from endocardium to epicardium was measured by cardiac magnetic resonance perfusion imaging (CMR-PI) in a dog during adenosine vasodilation with a severe stenosis of the left circumflex coronary artery. A plot profile taken through the anteroseptum and inferolateral wall over time resembles the M-mode display in echocardiography. Time-intensity curves measured in 2-voxel increments demonstrate a progressive reduction in flow from epicardium to endocardium in the inferolateral stenosis zone and relatively uniform flow in the anteroseptal remote zone. Reprinted with permission from Lee et al. (54). AUC = area under the curve; LV = left ventricle; RV = right ventricle.

The development of accurate automated contour detection algorithms remains a challenging issue, and significant user interaction is still required to ensure consistently accurate TICs—especially when poor breatholding results in cardiac motion. Furthermore, calculation of AMBF requires specialized computational software to obtain the transfer function from the LV and myocardial TICs. Software capable of automatic AMBF calculation will be necessary for this technique to move beyond the research realm.

Conclusions

AMBF can be calculated by mathematical modeling of CMR-PI studies. AMBF is more accurate than semiquantitative or qualitative methods for identifying hemodynamically significant coronary artery stenoses in experimental models and patients with suspected CAD. The ability to detect global reductions in perfusion reserve, assess serial changes in flow with improved precision, and examine subendocardial flow can provide important insights to our understanding of the pathophysiology of myocardial disease and aid in the evaluation of novel therapies.

Reprint requests and correspondence: Dr. Daniel C. Lee, 303 East Chicago Avenue, Tarry 14-725, Chicago, Illinois 60611. *Email: dlee@northwestern.edu.*

REFERENCES

1. White CW, Wright CB, Doty DB, et al. Does visual interpretation of the coronary arteriogram predict the physiologic importance of a coronary stenosis? N Engl J Med 1984;310:819–24.
2. Schelbert HR. Positron emission tomography of the heart: methodology, findings in the normal and diseased heart, and clinical applications. In: Phelps ME, PET Molecular Imaging and Its Biological Applications. New York: Springer-Verlag, 2004:433.
3. Smith AM, Gullberg GT, Christian PE. Experimental verification of technetium 99m-labeled teboroxime kinetic parameters in the myocardium with dynamic single-photon emission computed tomography: reproducibility, correlation to flow, and susceptibility to extravascular contamination. J Nucl Cardiol 1996;3:130–42.
4. Wei K, Jayaweera AR, Firoozan S, Linka A, Skyba DM, Kaul S. Quantification of myocardial blood flow with ultrasound-induced destruction of microbubbles administered as a constant venous infusion. Circulation 1998;97:473–83.
5. George RT, Jerosch-Herold M, Silva C, et al. Quantification of myocardial perfusion using dynamic 64-detector computed tomography. Invest Radiol 2007;42:815–22.
6. Pennell DJ, Sechtem UP, Higgins CB, et al. Clinical indications for cardiovascular magnetic resonance (CMR): Consensus Panel report. Eur Heart J 2004;25:1940–65.
7. Nandalur KR, Dwamena BA, Choudhri AF, Nandalur MR, Carlos RC. Diagnostic performance of stress cardiac magnetic resonance imaging in the detection of coronary artery disease: a meta-analysis. J Am Coll Cardiol 2007;50:1343–53.
8. Lee DC, Klocke FJ. Magnetic resonance approaches and recent advances in myocardial perfusion imaging. Curr Cardiol Rep 2006;8:59–64.
9. Klocke FJ, Simonetti OP, Judd RM, et al. Limits of detection of regional differences in vasodilated flow in viable myocardium by first-pass magnetic resonance perfusion imaging. Circulation 2001;104:2412–6.
10. Kraitchman DL, Wilke N, Hexeberg E, et al. Myocardial perfusion and function in dogs with moderate coronary stenosis. Magn Reson Med 1996;35:771–80.

11. Nagel E, Klein C, Paetsch I, et al. Magnetic resonance perfusion measurements for the noninvasive detection of coronary artery disease. Circulation 2003;108:432–7.
12. Jahnke C, Nagel E, Gebker R, et al. Prognostic value of cardiac magnetic resonance stress tests: adenosine stress perfusion and dobutamine stress wall motion imaging. Circulation 2007; 115:1769–76.
13. Klocke FJ, Baird MG, Lorell BH, et al. ACC/AHA/ASNC guidelines for the clinical use of cardiac radionuclide imaging—executive summary: a report of the American College of Cardiology/American Heart Association Task Force on Practice Guidelines (ACC/AHA/ASNC Committee to Revise the 1995 Guidelines for the Clinical Use of Cardiac Radionuclide Imaging). J Am Coll Cardiol 2003;42: 1318–33.
14. Axel L. Tissue mean transit time from dynamic computed tomography by a simple deconvolution technique. Invest Radiol 1983;18:94–9.
15. Jerosch-Herold M, Wilke N, Stillman AE. Magnetic resonance quantification of the myocardial perfusion reserve with a Fermi function model for constrained deconvolution. Med Phys 1998;25:73–84.
16. Gatehouse PD, Elkington AG, Ablitt NA, Yang GZ, Pennell DJ, Firmin DN. Accurate assessment of the arterial input function during high-dose myocardial perfusion cardiovascular magnetic resonance. J Magn Reson Imaging 2004;20:39–45.
17. Christian TF, Rettmann DW, Aletras AH, et al. Absolute myocardial perfusion in canines measured by using dual-bolus first-pass MR imaging. Radiology 2004;232:677–84.
18. Christian TF, Aletras AH, Arai AE. Estimation of absolute myocardial blood flow during first-pass MR perfusion imaging using a dual-bolus injection technique: comparison to single-bolus injection method. J Magn Reson Imaging 2008;27:1271–7.
19. Vallee JP, Sostman HD, MacFall JR, et al. MRI quantitative myocardial perfusion with compartmental analysis: a rest and stress study. Magn Reson Med 1997;38:981–9.
20. Utz W, Niendorf T, Wassmuth R, Messroghli D, Dietz R, Schulz-Menger J. Contrast-dose relation in first-pass myocardial MR perfusion imaging. J Magn Reson Imaging 2007;25:1131–5.
21. Lee DC, Johnson NP, O'Hara KC, Harris KR. Correcting the underestimation of absolute myocardial blood flow by magnetic resonance perfusion imaging. Circulation 2008;118: II_A33. Abstract 1081.
22. Cernicanu A, Axel L. Theory-based signal calibration with single-point T1 measurements for first-pass quantitative perfusion MRI studies. Acad Radiol 2006;13:686–93.
23. Hsu LY, Kellman P, Arai AE. Nonlinear myocardial signal intensity correction improves quantification of contrast-enhanced first-pass MR perfusion in humans. J Magn Reson Imaging 2008;27:793–801.
24. Calamante F. Bolus dispersion issues related to the quantification of perfusion MRI data. J Magn Reson Imaging 2005;22:718–22.
25. Jerosch-Herold M, Hu X, Murthy NS, Seethamraju RT. Time delay for arrival of MR contrast agent in collateral-dependent myocardium. IEEE Trans Med Imaging 2004;23:881–90.
26. Thompson HK Jr., Starmer CF, Whalen RE, McIntosh HD. Indicator transit time considered as a gamma variate. Circ Res 1964;14:502–15.
27. Jerosch-Herold M, Swingen C, Seethamraju RT. Myocardial blood flow quantification with MRI by model-independent deconvolution. Med Phys 2002;29:886–97.
28. Larsson HB, Stubgaard M, Sondergaard L, Henriksen O. In vivo quantification of the unidirectional influx constant for Gd-DTPA diffusion across the myocardial capillaries with MR imaging. J Magn Reson Imaging 1994;4:433–40.
29. Mühling OM, Wang Y, Panse P, et al. Transmyocardial laser revascularization preserves regional myocardial perfusion: an MRI first pass perfusion study. Cardiovasc Res 2003;57:63–70.
30. Heymann MA, Payne BD, Hoffman JI, Rudolph AM. Blood flow measurements with radionuclide-labeled particles. Prog Cardiovasc Dis 1977; 20:55–79.
31. Jerosch-Herold M, Wilke N. MR first pass imaging: quantitative assessment of transmural perfusion and collateral flow. Int J Card Imaging 1997;13:205–18.
32. Wilke N, Jerosch-Herold M, Wang Y, et al. Myocardial perfusion reserve: assessment with multisection, quantitative, first-pass MR imaging. Radiology 1997;204:373–84.
33. Vallee JP, Sostman HD, MacFall JR, et al. Quantification of myocardial perfusion by MRI after coronary occlusion. Magn Reson Med 1998;40: 287–97.
34. Muehling OM, Jerosch-Herold M, Panse P, et al. Regional heterogeneity of myocardial perfusion in healthy human myocardium: assessment with magnetic resonance perfusion imaging. J Cardiovasc Magn Reson 2004; 6:499–507.
35. Hsu LY, Rhoads KL, Holly JE, Kellman P, Aletras AH, Arai AE. Quantitative myocardial perfusion analysis with a dual-bolus contrast-enhanced first-pass MRI technique in humans. J Magn Reson Imaging 2006;23:315–22.
36. Wilson RF, Wyche K, Christensen BV, Zimmer S, Laxson DD. Effects of adenosine on human coronary arterial circulation. Circulation 1990;82: 1595–606.
37. Chareonthaitawee P, Kaufmann PA, Rimoldi O, Camici PG. Heterogeneity of resting and hyperemic myocardial blood flow in healthy humans. Cardiovasc Res 2001;50:151–61.
38. Costa MA, Shoemaker S, Futamatsu H, et al. Quantitative magnetic resonance perfusion imaging detects anatomic and physiologic coronary artery disease as measured by coronary angiography and fractional flow reserve. J Am Coll Cardiol 2007;50:514–22.
39. Futamatsu H, Wilke N, Klassen C, et al. Evaluation of cardiac magnetic resonance imaging parameters to detect anatomically and hemodynamically significant coronary artery disease. Am Heart J 2007;154:298–305.
40. Al-Saadi N, Nagel E, Gross M, et al. Noninvasive detection of myocardial ischemia from perfusion reserve based on cardiovascular magnetic resonance. Circulation 2000;101:1379–83.
41. Petersen SE, Jerosch-Herold M, Hudsmith LE, et al. Evidence for microvascular dysfunction in hypertrophic cardiomyopathy: new insights from multiparametric magnetic resonance imaging. Circulation 2007;115: 2418–25.
42. Muehling OM, Wilke NM, Panse P, et al. Reduced myocardial perfusion reserve and transmural perfusion gradient in heart transplant arteriopathy assessed by magnetic resonance imaging. J Am Coll Cardiol 2003;42: 1054–60.
43. Wang L, Jerosch-Herold M, Jacobs DR Jr., Shahar E, Folsom AR. Coronary risk factors and myocardial perfusion in asymptomatic adults: the Multi-Ethnic Study of Atherosclerosis (MESA). J Am Coll Cardiol 2006; 47:565–72.
44. Wang L, Jerosch-Herold M, Jacobs DR Jr., Shahar E, Detrano R, Folsom AR. Coronary artery calcification and myocardial perfusion in asymptomatic adults: the MESA (Multi-Ethnic Study of Atherosclerosis). J Am Coll Cardiol 2006;48:1018–26.
45. Rosen BD, Lima JA, Nasir K, et al. Lower myocardial perfusion reserve is associated with decreased regional left ventricular function in asymptomatic participants of the multi-ethnic study of atherosclerosis. Circulation 2006; 114:289–97.

JACC: CARDIOVASCULAR IMAGING, VOL. 2, NO. 6, 2009
JUNE 2009:761–70

46. Panse P, Klassen C, Panse N, et al. Magnetic resonance quantitative myocardial perfusion reserve demonstrates improved myocardial blood flow after angiogenic implant therapy. Int J Cardiovasc Imaging 2007;23:217–24.
47. Selvanayagam JB, Jerosch-Herold M, Porto I, et al. Resting myocardial blood flow is impaired in hibernating myocardium: a magnetic resonance study of quantitative perfusion assessment. Circulation 2005;112:3289–96.
48. Selvanayagam JB, Cheng AS, Jerosch-Herold M, et al. Effect of distal embolization on myocardial perfusion reserve after percutaneous coronary intervention: a quantitative magnetic resonance perfusion study. Circulation 2007;116:1458–64.
49. Elkington AG, Gatehouse PD, Ablitt NA, Yang GZ, Firmin DN, Pennell DJ. Interstudy reproducibility of quantitative perfusion cardiovascular magnetic resonance. J Cardiovasc Magn Reson 2005;7:815–22.
50. Jerosch-Herold M, Vazquez G, Wang L, Jacobs DR Jr., Folsom AR. Variability of myocardial blood flow measurements by magnetic resonance imaging in the multi-ethnic study of atherosclerosis. Invest Radiol 2008;43:155–61.
51. Chareonthaitawee P, Christenson SD, Anderson JL, et al. Reproducibility of measurements of regional myocardial blood flow in a model of coronary artery disease: comparison of H215O and 13NH3 PET techniques. J Nucl Med 2006;47:1193–201.
52. Kaufmann PA, Gnecchi-Ruscone T, Yap JT, Rimoldi O, Camici PG. Assessment of the reproducibility of baseline and hyperemic myocardial blood flow measurements with 15O-labeled water and PET. J Nucl Med 1999;40:1848–56.
53. Chilian WM. Microvascular pressures and resistances in the left ventricular subepicardium and subendocardium. Circ Res 1991;69:561–70.
54. Lee DC, Simonetti OP, Harris KR, et al. Magnetic resonance versus radionuclide pharmacological stress perfusion imaging for flow-limiting stenoses of varying severity. Circulation 2004;110:58–65.
55. Panting JR, Gatehouse PD, Yang GZ, et al. Abnormal subendocardial perfusion in cardiac syndrome X detected by cardiovascular magnetic resonance imaging. N Engl J Med 2002;346:1948–53.
56. Knowles BR, Batchelor PG, Parish V, et al. Pharmacokinetic modeling of delayed gadolinium enhancement in the myocardium. Magn Reson Med 2008;60:1524–30.

Key Words: blood flow quantification ■ cardiac magnetic resonance ■ gadolinium ■ myocardial perfusion ■ quantitative modeling.